# Energetics and local vibrations of the *DX* center in GaAs

Mineo Saito
*NEC Scientific Information System Development, Ltd., 34 Miyukigaoka, Tsukuba, Ibaraki 305, Japan*

Atsushi Oshiyama and Osamu Sugino
*Microelectronics Research Laboratories, NEC Corporation, 34 Miyukigaoka, Tsukuba, Ibaraki 305, Japan*
(Received 28 September 1992; revised manuscript received 15 December 1992)

The negatively charged broken-bond geometry is a strong candidate for the microscopic origin of the *DX* center in GaAs but the validity of the broken-bond model is still controversial. We thus examine the model for the Si-related *DX* center, performing large-scale supercell calculations within the local-density approximation. The highly efficient conjugate-gradient minimization technique is combined with the norm-conserving-pseudopotential method in order to include both short-range and medium-range lattice relaxations. First, we compare the total energy of the broken-bond geometry with that of the negatively charged on-site geometry, which is also a candidate for the *DX* center. It is found that the broken-bond geometry has a lower total energy, supporting the broken-bond model for the *DX* center. Second, the barrier height for the broken-bond geometry is found to be comparable to observed emission barriers for the *DX* center. Third, the broken-bond model is shown to be consistent with results of a Fourier-transform infrared-absorption measurement for the local vibrational frequency of Si in pressurized GaAs, although the neutral on-site model also reproduces the experimental results within the calculational accuracy. Most of the results in this work indicate that the broken-bond model is consistent with experiments. Finally, we find that the broken-bond model with the neutral charge state is unstable and thus expect that the Si atom moves to the substitutional site after the *DX* center is photoexcited.

## I. INTRODUCTION

Both group-IV and group-VI atoms induce deep levels (*DX* levels) in $Al_xGa_{1-x}As$ ($x \geq 0.22$) alloy semiconductors and in pressurized GaAs, and exhibit physically interesting and technologically important properties.[1] The *DX* centers have barriers for both electron emission and capture, leading to persistent photoconductivity. There is a large Stokes shift between thermal and optical ionization energies.[2] It is now confirmed that the *DX* centers arise from donor impurities by themselves[3–16] and thus the *DX* center exhibits bistability with the typical shallow state in the semiconductors. Although a variety of models have been proposed for the *DX* center in order to explain the above observed results,[17–29] the origin of the *DX* center is not sufficiently revealed. Two points are now particularly controversial: whether the *DX* center is a positive- or negative-*U* center, and whether the *DX* center is accompanied with small lattice relaxation or with large lattice relaxation.

The broken-bond model proposed by Chadi and Chang (CC) (Ref. 25) from a supercell calculation based on the local-density approximation (LDA), is a strong candidate for the *DX* center. In the model for the Si-related *DX* center, one Si—As bond is broken by the displacement of the Si atom along the $[\bar{1}\,\bar{1}\,\bar{1}]$ axis and the other three Si—As bonds remain. CC argued that this broken-bond geometry is a minimum in total energy only when it is negatively charged, indicating that the *DX* center is a negative-*U* center. This model is shown to be consistent[25–27] with various experiments. However, the model is not completely supported by other theoretical studies based on LDA calculations. Large-scale supercell calculations are performed by Dabrowski, Scheffler, and Stehlow (DSS) (Ref. 28) and by Yamaguchi, Shiraishi, and Ohno (YSO).[29] YSO found that the negatively charged broken-bond geometry is metastable: The broken-bond geometry has higher energy than the negatively charged on-site geometry. They thus proposed the neutral on-site model in which a localized $a_1$ state appears in the energy gap. On the contrary, the total-energy calculation of DSS shows that the broken-bond model rather than the neutral on-site model is favorable. DSS, however, found a shallow barrier (less than 0.1 eV) for the neutral broken-bond geometry. This finding is inconsistent with the result of CC that the neutral broken-bond geometry is unstable. The discrepancy among the conclusions of CC, YSO, and DSS is discussed by Baraff.[30] Yet the origin of the discrepancy is still unclear. Jones and Öberg[31] argued from a cluster calculation that the energies of the negatively charged on-site and broken-bond geometries are close to each other, indicating that both geometries coexist in a sample. They conclude that the experimentally observed local vibrational mode[32] under high pressure is a mode in the negatively charged on-site geometry, while they also suggest the possibility that a mode in the neutral on-site geometry is the observed mode.

In a previous paper,[33] we reported results of 32-site supercell calculation within the LDA. We found several evidences supporting the broken-bond model for the group-IV atom induced *DX* center in GaAs. First, there exist several metastable geometries accompanied with large lattice relaxation other than the broken-bond

 

geometry but they have 0.6–0.9 eV higher total energies than the broken-bond geometry. Second, the local vibrational mode which is experimentally detected under high pressure is assigned to a Si-As bond-stretching $e$ mode in the broken-bond geometry. Third, the bond lengths between the group-IV donor and As atoms in the shallow and $DX$ centers are found to be *identical* to each other. This finding indicates that the broken-bond model is consistent with experimental results of an extended-x-ray-absorption-fine-structure (EXAFS) measurement[34] for Sn-doped GaAs.

In the present paper, we perform the thorough total-energy calculations using larger-size supercells that enable us to assess the importance of both short- and medium-range lattice relaxations. We have examined a variety of atomic geometries, including the negatively charged on-site geometry, and report detailed features of the successful model for the $DX$ center. The supercell calculations are performed using the norm-conserving pseudopotential method[35] within the LDA. In order to perform large-scale calculations, we combine the conjugate-gradient (CG) minimization technique[36] with the norm-conserving pseudopotential method. The accuracy of the obtained results are examined performing calculations with various sizes: The cell size is enlarged up to 64 sites and the cutoff energy of the plane-wave basis set up to 16 Ry is used. The medium-range lattice relaxation around the impurity is taken into account by relaxing all the atoms in the supercell (relaxation of more than 50 atoms). The important findings for GaAs:Si are as follows: The total energy of the negatively charged broken-bond geometry in GaAs, which was shown to be the most stable among the geometries with large lattice relaxation, is slightly lower than that of the negatively charged on-site geometry, supporting the broken-bond model. We will not compare the total energy with that of the substitutional geometry inducing the shallow level since the supercell LDA calculation is unlikely to provide the reliable total energy for the shallow state. The calculated emission barrier for the broken-bond geometry is comparable with the observed value for the $DX$ center. It is found that the $e$ local vibrational mode in the broken-bond geometry is a strong candidate for the observed mode under high pressures, though the frequency of the $t_2$ local vibrational mode in the neutral on-site geometry is also consistent with the experimental value within the calculational accuracy. Most of the present results support the broken-bond geometry. Finally, the neutral broken-bond geometry is found to be unstable, suggesting that the Si atom moves to the substitutional site after the $DX$ center is photoexited. Of note is that the above results are obtained by taking into account both short- and medium-range lattice relaxations.

In Sec. II we present the calculational method, and then examine the accuracy of the calculation by varying calculational parameters in Sec. III. In Sec. IV the results are presented, and conclusions are given in Sec. V.

## II. METHOD

In this section we give a brief description of the calculational method and then examine the accuracy of the present calculations in the next section. The supercell calculations are performed applying the norm-conserving pseudopotential method[35] based on the LDA. In order to perform large-scale calculations, we use the CG minimization technique[36] both for the electron degree of freedom and for the nucleus degree of freedom. The total-energy optimizations with respect to the electron and nucleus degrees of freedom are performed alternatively: we do not adopt the simultaneous minimization technique.[37] The computational procedure consists of threefold loops. In the innermost loop, the eigenfunctions $\{\psi_n\}$ are obtained for the Hamiltonian $H(\rho)$, which is a functional of a given electron density $\rho$:

$$[H(\rho)-\epsilon_n]\psi_n=0 , \tag{1}$$

where $\epsilon_n$ is the eigenvalue. Details for this loop are explained later. In the middle loop, we first choose an initial electron density and finally obtain the self-consistent electron density. In each iteration in the middle loop, the Hamiltonian $H(\rho^i)$ is first constructed from the input electron density ($\rho^i$), where $i$ indicates the iteration number. Second, the eigenfunctions ($\psi_n^{(i)}$) for this Hamiltonian are obtained in the innermost loop. Third, the output electron density ($\rho^i_{\text{output}}$) is constructed from the eigenfunctions:

$$\rho^i_{\text{output}}=\sum_n^{\text{occupied}} 2|\psi_n^{(i)}|^2 . \tag{2}$$

The input electron density $\rho^{i+1}$ in the next step is determined from $\rho^i_{\text{output}}$ based on an extrapolation scheme. The iteration in the middle loop is terminated if the input electron density $\rho^i$ and the output electron density $\rho^i_{\text{output}}$ are close to each other within the calculational accuracy. In the outermost loop, the force acting on each atom is calculated from the obtained self-consistent electron density and the geometry in which all the forces are zero is searched. The CG method is applied to the innermost and outermost loops.

The procedure in the innermost loop is as follows. Solving (1) for a given $\rho^i$ is equivalent to searching the wave functions $\psi_n$, which give the zero value of the following quantity:

$$D_n=[H(\rho^i)-\langle\psi_n|H(\rho^i)|\psi_n\rangle]\psi_n . \tag{3}$$

In the $k$th iterative step toward such $\{\psi_n\}$, we calculate $D_n^k$ in (3) for the wave function $\psi_n^k$, and then determine the new set of wave functions $\{\psi_n^{k+1}\}$ from $\{D_n^k\}$ by using the preconditioned CG method.[38] If we continue the iteration till $\{D_n^k\}$ are close to zero, $\{\psi_n^k\}$ become accurate eigenfunctions. In order to save computational time, however, we limit the iteration number to a small number: the iteration is terminated even when the exact eigenfunction for $H(\rho^i)$ is not obtained. Yet the exact eigenfunctions can be obtained finally by enough iterations for the self-consistent electron density, which is obtained, in turn, from the middle loop.

To save computational time in the CG calculation, we rewrite the norm-conserving pseudopotentials in separable forms.[39,40] In our previous study,[35] we constructed, nonseparable norm-conserving relativistic pseudopoten-

tials for Si, Ga, and As atoms. These pseudopotentials have the form

$$V=|0\rangle\delta v_0\langle 0|+|1\rangle\delta v_1\langle 1|+v_2 , \quad (4)$$

where $v_l$ is the nonlocal pseudopotential with the angular momentum $l$, $|l\rangle\langle l|$ is the projection into the $l$th component, and $\delta v_l=v_l-v_2$. In the above equation, we assume that $v_l=v_2$ for $l>2$. The Kleinman-Bylander approximation,[39] which replaces the term $\delta v_l$ in (4) by the following separable form, greatly reduces computational efforts:

$$\delta v_l'=\frac{|\phi\delta v_l\rangle\langle\delta v_l\phi|}{\langle\phi|\delta v_l|\phi\rangle} , \quad (5)$$

where $\phi$ is the atomic wave function of the $l$th component. This approximation is valid for the Si atom but raises a problem for, in particular, the $s$ parts ($\delta v_0$) in the Ga and As atoms.[41] We previously found that the real-space-partitioned pseudopotential method[40] is valid for this case. In the method, first, $\delta v_l$ is partitioned into two parts in the real space and, second, the separable form is constructed for each part:

$$\delta v_l''=\sum_{k=1}^{2}\frac{|\phi\Delta_k\rangle\langle\Delta_k\phi|}{\langle\phi|\Delta_k|\phi\rangle} , \quad (6)$$

where

$$\Delta_1=\frac{\delta v_l}{1+\exp[\beta(\alpha-r)]} \quad (7)$$

and $\Delta_2=\delta v_l-\Delta_1$. In a previous paper,[40] we have found that the real-space-partitioned separable pseudopotentials are reliable and work well when the partitioning point $\alpha$ is carefully chosen. In the present case, we take $\beta=5.0$ a.u.$^{-1}$ and $\alpha=1.0$ a.u. Numerical tests for these potentials of Ga and As are presented in Sec. III.

In order to examine accuracy of the present calculations, we perform calculations by varying calculational parameters. Each unit cell in the employed supercell models contains 16, 32, 54, or 64 lattice sites. The shape of the cell is a diamond type for the 16- and 54-site cells, rectangular parallelepiped for the 32-site cell and cubic for the 64-site cell. In performing the Brillouin-zone integration, we take 1 (2) special point(s) proposed by Baldereschi[42] (Chadi and Cohen[43]) for the 32- and 64- (16- and 54-) site cells. As a result, the total number of the sampling $k$ points in the Brillouin zone is 4 for the 32- and 64-site cells. The cutoff energy for the plane-wave basis set is taken from 8 to 16 Ry. Most of the calculations are performed for the case of zero pressure: the lattice constant of GaAs is taken to be 5.65 Å, which is an experimental value.

Both short- and medium-range relaxations of the atoms occur around the impurity atom. These relaxations play an important role in the energetics of the impurity in semiconductors. In order to take into account this effect, we optimize the geometry by relaxing all the atoms in the cell. The remaining force acting on each atom is less than 0.5 mRy/a.u. after the geometry optimization.

TABLE I. Eigenvalue of the lowest conduction band of GaAs at several high-symmetry points, calculated by using the relativistic separable pseudopotentials within the LDA. The real-space-partitioned pseudopotential method is applied to the $s$ parts of pseudopotentials for Ga and As atoms. The values in parentheses are obtained using the original nonseparable pseudopotential. The employed cutoff energies $E_{\text{cutoff}}$ are 8–20 Ry: The eigenvalues are measured in eV from the valence-band top.

| $E_{\text{cutoff}}$ | $\Gamma$ | $X$ | $L$ |
|---|---|---|---|
| 8 | 1.950 (1.970) | 1.758 (1.782) | 1.838 (1.851) |
| 12 | 1.396 (1.364) | 1.451 (1.440) | 1.299 (1.262) |
| 16 | 0.777 (0.702) | 1.411 (1.390) | 1.124 (1.073) |
| 20 | 0.743 (0.671) | 1.405 (1.385) | 1.105 (1.054) |

## III. ACCURACY OF CALCULATION

In this section we examine the accuracy of the present calculational method. First we study the validity of the real-space-partitioned method which is applied to the $s$ parts of the pseudopotentials of Ga and As. For this purpose, results from the real-space-partitioned separable pseudopotentials and from the original nonseparable pseudopotentials are compared. In Table I we tabulate the calculated eigenvalues of the lowest conduction band in GaAs. It is found that the real-space-partitioned method successfully reproduces the results from the nonseparable pseudopotentials within an accuracy of 0.07 eV for various values (8–20 Ry) of the cutoff energy for the plane-wave basis set. Next, the ground-state properties of GaAs are calculated with the 20-Ry cutoff energy. We find that the method reproduces results from the original nonseparable pseudopotential: The lattice constant and the transverse optical (TO) phonon frequency $\omega_{\text{TO}}$ at the $\Gamma$ point are reproduced within accuracies of 0.01 Å and 1 cm$^{-1}$, respectively (Table II). It is thus concluded that there is no problem in using the present separable pseudopotentials instead of the original nonseparable pseudopotentials.

TABLE II. Ground-state properties of Si and GaAs. The calculations are performed by using the separable pseudopotentials with the cutoff energy of 20 Ry. As for the $s$ parts of the Ga and As atoms, the real-space-partitioned potential method is applied. The values in parentheses are obtained by using the original nonseparable pseudopotentials.

| | | Lattice constant[a] | Bond length[a] | $\omega_{\text{TO}}$[b] |
|---|---|---|---|---|
| Si | theory | 5.40 | 2.34 | 500 |
| | experiment | 5.43 | 2.35 | 517[c] |
| GaAs | theory | 5.62 | 2.43 | 256 |
| | | (5.61) | (2.43) | (257) |
| | experiment | 5.65 | 2.45 | 271[d] |

[a]In Å.
[b]In cm$^{-1}$.
[c]Reference 44.
[d]Reference 45.

Second, we discuss how well the LDA calculations with the present separable pseudopotentials reproduce experimental results for the ground-state properties of Si and GaAs crystals. The cutoff energy used in these calculations is taken to be 20 Ry, which provides the converged results. It is found that the bond lengths and $\omega_{TO}$ are reproduced for both crystals within accuracies of 0.01 Å and 5.5% (Table II), respectively. Thus second derivatives of the total energy with respect to nuclear coordinates are expected to be obtained within an accuracy of 5.5% from the present LDA calculations.

It is found from the above examination that the bond lengths and the second derivatives of the total energy with respect to the nuclear coordinate are reliable if the cutoff energy of 20 Ry is taken. However, in actual supercell calculations, smaller cutoff energies are favored in order to save computational time. The deviation arising from the calculation with the smaller cutoff energies should thus be investigated. For this purpose, we calculate the ground-state properties of Si and GaAs crystals by varying the cutoff energy. We first distort the two atoms in each unit cell in the opposite directions along the [100] axis: the amounts of distortion are 0.69 and 0.71 Å for Si and GaAs, respectively. The calculated distortion energy $\delta E$ is shown in Table III. The results with the cutoff energies ranging from 8 to 20 Ry agree within 0.1 eV in both crystals. It is thus expected that the calculation with use of 8-Ry cutoff energy reproduces potential-energy surfaces within an accuracy of 0.1 eV. However, the calculated $\omega_{TO}$ from the 8-Ry cutoff energy deviates 6% and 11% from the converged values in GaAs and Si, respectively. Thus calculation with 8 Ry as the cutoff energy is not reliable for the second derivative of the total energy with respect to nuclear coordinates. In order to reduce the deviation to within 2%, we need to use 12 Ry for the cutoff energy.

Finally, we investigate the size effect of the supercell model. For this purpose, we compare the energy difference between two geometries of the positively charged Si impurity in GaAs. In one geometry, Si is situated at the substitutional site, and in the other geometry, Si is displaced by 1.42 Å along the $[\bar{1}\,\bar{1}\,\bar{1}]$ axis. The relaxation of the other atoms is not considered, and the cutoff energy is taken to be 8 Ry for the present purpose. It is found that the energy difference is 3.00, 3.21, and 3.11 eV for 16-, 32-, and 54-site unit cells, respectively. Thus the calculations with these cells seem to induce the deviation less than 0.1 eV. However, the difference in optimized geometry among the three unit cells is not considered in the above discussion: the difference is expected to occur because of the medium-range relaxation, so the total energy of the optimized geometry may be different. Further examination of the cell size effect is performed in Sec. IV by comparing results from the 32- and 64-site cell models.

## IV. RESULTS AND DISCUSSION

In this section we present the detailed results of the total-energy calculations for several geometries of GaAs:Si. The results provide the energetics of the Si impurity in GaAs and validate the broken-bond model for the *DX* center.

### A. Broken-bond model: $(Si_I V_{Ga})^{-1}$

We begin with the negatively charged broken-bond geometry $(Si_I V_{Ga})^{-1}$. First, the accuracy of the calculation is examined by varying cell size and cutoff energy (Table IV). We perform the 32-site cell calculations with 8- and 12-Ry cutoff energies and the 64-site cell calculations with 8- and 10-Ry cutoff energies. All these calculations provide results which are close to each other: The results for the Si-As bond length agree within an accuracy of 0.01 Å and those for the optimized angles between the Si—As bonds agree within an accuracy of 1°. Thus the results for the geometry are expected to be converged for the cell size and cutoff energy.

We then present characteristic features of the optimized broken-bond geometry obtained from the 64-site calculation with 10-Ry cutoff energy. In the optimized geometry, the Si atom is distorted from the lattice site by 1.40 Å along the $[\bar{1}\,\bar{1}\,\bar{1}]$ axis, and the angle between Si—As bonds becomes 115°. The amount of the distortion is 57% of the crystal bond length (2.45 Å) and thus the Si atom passes the "$sp^2$ hybridization point," where the Si and nearest three As atoms become coplanar (the amount of the distortion in the coplanar geometry is 33% of the crystal bond length if the As atoms are not relaxed). The medium-range relaxation of atoms along the zigzag chain

TABLE III. The TO phonon frequency $\omega_{TO}$ at the Γ point and the energy cost $\delta E$ by the distortion along the [001] axis (each of the two atoms in every unit cell is distorted in the opposite direction by 0.69 and 0.71 Å in Si and GaAs, respectively). The calculations are performed by using the separable pseudopotentials with cutoff energies $E_{cutoff}$ from 8 to 20 Ry.

| | $E_{cutoff}$[a] | 8 | 12 | 16 | 20 |
|---|---|---|---|---|---|
| Si | $\omega_{TO}$[b] | 555 | 512 | 506 | 500 |
| | $\delta E$[c] | 4.86 | 4.89 | 4.86 | 4.81 |
| GaAs | $\omega_{TO}$ | 241 | 253 | 256 | 256 |
| | $\delta E$ | 1.73 | 1.62 | 1.64 | 1.64 |

[a]In Ry.
[b]In $cm^{-1}$.
[c]In eV.

TABLE IV. Optimized geometries of $D^0$, $(Si_I V_{Ga})^{-1}$, and $(Si_{Ga})^{-1}$. The Si-As bond lengths $l_{Si\text{-}As}$, displacements of Si along the $[\bar{1}\bar{1}\bar{1}]$ axis, $\delta^{b}_{\|[\bar{1}\bar{1}\bar{1}]}$, and Si-As bond angles $\theta$ are tabulated. $\Delta E$ is the energy of the negatively charged on-site geometry measured from that of the broken-bond geometry under zero pressure. The $n_{site}$ site cell is used in the supercell calculations with the cutoff energy $E_{cutoff}$.

| | | $(Si_I V_{Ga})^{-1}$ | | | $(Si_{Ga})^{-1}$ | $D^0$ | |
|---|---|---|---|---|---|---|---|
| $n_{site}$ | $E_{cutoff}$[a] | $l_{Si\text{-}As}$[b] | $\delta_{\|[\bar{1}\bar{1}\bar{1}]}$[b] | $\theta$[c] | $l_{Si\text{-}As}$ | $l_{Si\text{-}As}$ | $\Delta E$[d] |
| 32 | 8 | 2.42 | 1.39 | 114 | 2.46 | 2.42 | 0.16 |
| | 12 | 2.42 | 1.41 | 115 | 2.46 | 2.43 | 0.25 |
| | 16 | | | | | | 0.27[e] |
| 64 | 8 | 2.41 | 1.37 | 115 | 2.56 | 2.41 | 0.31 |
| | 10 | 2.41 | 1.40 | 115 | 2.53 | 2.41 | 0.27 |

[a]In Ry.
[b]In Å.
[c]In degrees.
[d]In eV.
[e]$\Delta E$ is obtained for the geometries optimized from the 32-site cell calculation with 8-Ry cutoff energy.

on the $(1\bar{1}0)$ plane is shown in Fig. 1. The displacements from the lattice site of the first-, second-, and third-nearest atoms of the Si atom along the zigzag chain are found to be 0.05, 0.02, and 0.02 Å, respectively. The distortion of the fourth-nearest Ga atom, which is at a boundary site in the 64-site cell, is less than 0.005 Å. As Fig. 1 shows, the Ga-As bond length between the first- and second-nearest atoms and the one between the second- and third-neighbor atoms are close to the crystal bond length (2.45 Å). It is noted that the bond angle at the first-nearest As atom is 75.7° and that the distance between the Si and the second-nearest Ga atoms is very short (2.98 Å). Thus there is a weak interaction between the Si and Ga atoms, though there seems to be no bond charge between the two atoms (Fig. 2). It is noted that this weak interaction is expected to cause the local-alloy effect: If second-nearest Ga atoms are replaced by Al atoms in $Al_xGa_{1-x}As$, the energy of the broken-bond geometry shifts. The remaining As atom, which is separated from the Si impurity and threefold coordinated, is distorted by 0.14 Å in the direction of the $[\bar{1}\bar{1}\bar{1}]$ axis. The first-nearest Ga atom of this As atom is also displaced by 0.05 Å. As a result, the Ga-As bond length is 0.05 Å shorter than the crystal value, indicating that this bond is strengthened. The bond angles between each two of the three Ga—As bonds are 105°, which is smaller than the $sp^3$ hybridization angle (109.5°). The second-neighbor As atom of the threefold-coordinated As atom is distorted by 0.02 Å, and the bond length between the first- and second-nearest atoms is the same as the crystal bond length.

There is a small but important difference in the optimized geometry of CC and us: CC estimate the displacement of the Si atom and the Si-As bond angle to be 1.17 Å and 118.4°, respectively. Since this bond angle is close to 120°, CC considered that the hybridization character in the Si atom is $sp^2$. In the geometry optimized in this

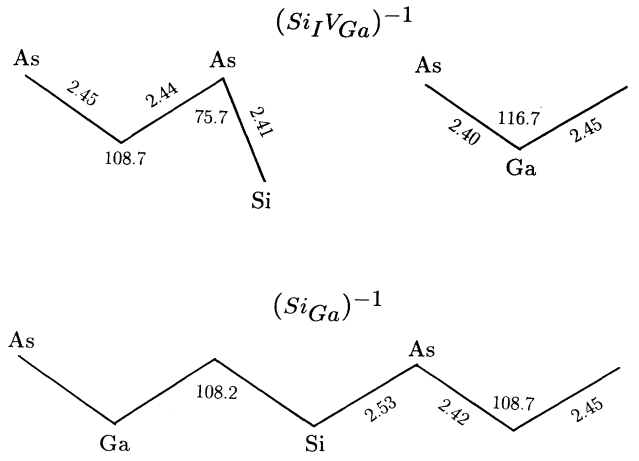


FIG. 1. Atomic configurations of $(Si_I V_{Ga})^{-1}$ and $(Si_{Ga})^{-1}$ on the $(1\bar{1}0)$ plane. Bond lengths are in Å and bond angles are in degrees.

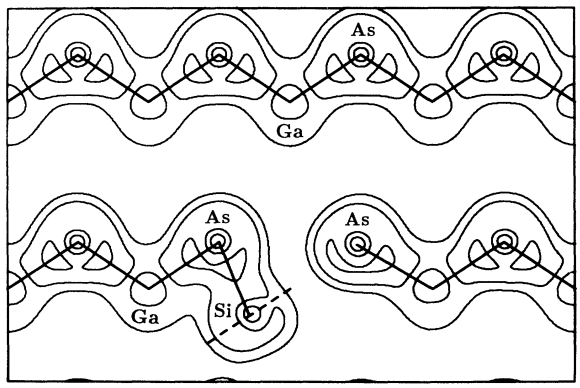


FIG. 2. The total valence electron density in $(Si_I V_{Ga})^{-1}$ on the $(1\bar{1}0)$ plane. The values of the contours are $0.08\times2^n$ $e$/(a.u.)$^3$, where $n=0$–2. The dashed line is parallel to the [111] axis.

paper, however, the displacement of the Si atom is 0.23 Å larger and, consequently, the Si-As bond angle is smaller (115°), compared with the geometry by CC. From the calculated bond angle in the present geometry, the hybridization character for the Si—As bond is estimated to be $sp^{2.4}$, which is between $sp^2$ and $sp^3$ (see the Appendix). Consequently, the lone pair electrons in the Si atom occupy a $s$-$p$ hybridized dangling bond orbital whose character is between the $p_\pi$ nonbonding orbital and $sp^3$ dangling-bond orbital. As is shown in Fig. 2, the charge density around the Si atom is relatively high in the direction of the $[\bar{1}\,\bar{1}\,\bar{1}]$ axis, while the density is low in the opposite direction. This antisymmetric charge distribution along the [111] axis is due to the fact that the lone pair electrons occupy the $s$-$p$ hybridized dangling-bond orbital:[46] When the lone pair electrons occupy the pure $p_\pi$ orbital, they contribute to a symmetric charge distribution. The energy gain induced by the variation from the $sp^2$ planar to the $sp^{2.4}$ nonplanar structures is presumably due to the fact that the energy of the dangling-bond orbital in the latter structure is lower than that of the nonbonding $p_\pi$ orbital in the former structure (since the dangling orbital contains the $s$ component, the orbital energy is lower than that of the $p_\pi$ orbital). A similar situation is found for the $NH_3$ molecule, where the N atom is threefold coordinated: the planar geometry ($sp^2$ structure) of this molecule is unstable and the nonplanar geometry ($sp^3$-like structure) is the most stable.

### B. On-site model: $(Si_{Ga})^{-1}$

We next study the negative on-site geometry $(Si_{Ga})^{-1}$. The 32-site cell calculations with 8- and 12-Ry cutoff energies lead to the result that the Si-As bond length is 2.46 Å (Table IV). On the other hand, the longer bond lengths (2.53–2.56 Å) are obtained from the 64-site calculation with 8- and 10-Ry cutoff energies, indicating that the bond length is prolonged by the long-range relaxation around the Si atom. The results of the calculation with 10-Ry cutoff energy are expected to be almost converged from our experiences of supercell calculations.[47]

We then report the optimized atomic structure obtained from the calculation with 10-Ry cutoff energy. The optimized Si-As bond length is 2.53 Å, which is much longer than that of the broken-bond geometry (2.41 Å). The obtained longer bond length is due to the fact that the gap level has the wave function whose amplitude is localized around the Si atom and has antibonding character: The wave function has indeed a node between the Si and As atoms (see Fig. 3). In Fig. 1, we show the atomic configuration of the zigzag chain on the $(1\bar{1}0)$ plane. The displacements of the first, second, and third neighbor atoms are 0.08, 0.02, and 0.02 Å from the lattice sites, respectively. As a result, the Ga-As bond lengths are 2.42 and 2.45 Å between the first- and second-nearest atoms and between the second- and the third-nearest atoms, respectively: These values are close to that of the crystal bond length. Since the wave function of the gap level is localized around the Si atom, the electrons in the gap level only slightly affect these Ga—As bonds around the Si atom.

Next, the total-energy difference $\Delta E$ between the optimized broken-bond and on-site geometries is calculated (Table IV): $\Delta E$ is the energy of the negatively charged on-site geometry measured from that of the broken-bond geometry. First we perform 32-site cell calculations. When the cutoff energy is taken to be 8 Ry, $\Delta E$ is 0.16 eV. When the cutoff energy is increased to be 12 Ry, $\Delta E$ becomes 0.25 eV. Yet, the optimized geometries from $E_{\text{cutoff}}=8$ and 12 Ry are close to each other. If we calculate the energy difference with $E_{\text{cutoff}}=16$ Ry at the geometry optimized from the calculation with $E_{\text{cutoff}}=8$ Ry, $\Delta E$ increases by 0.11 eV compared with the calculated $\Delta E$ and $E_{\text{cutoff}}=8$ Ry. Thus, although the calculation with 8-Ry cutoff energy provides the converged result for the atomic geometry, there arises the deviation of $\Delta E$ by about 0.1 eV. This deviation from the use of 8-Ry cutoff energy is expected from our experiences described in Sec. III (Table III). We next perform 64-site cell calculations. The calculations with 8- and 10-Ry cutoff energies lead to results of $\Delta E=0.31$ and 0.27 eV, respectively. We expect from the experiences of the 32-site cell calculations and of the check calculations in Sec. III that the value of $\Delta E$ from the 64-site cell calculation with 8- or 10-Ry cutoff energy deviates by at most 0.1 eV from the converged value with respect to the cutoff energy. Even if the present value (0.27 eV) deviates by this maximum amount, however, $\Delta E$ is still positive. It is thus concluded that the broken-bond model has lower energy than the on-site model under ambient pressure. The pressure effect on the value of $\Delta E$ is studied using the 32-site calculation with 12-Ry cutoff energy. It is found that the value of $\Delta E$ is insensitive to the pressure: $\Delta E$ decreases by only 0.06 eV when pressure of 21 kbar is applied. Thus the sign of $\Delta E$ is positive in high pressures which induce the $DX$ level in the gap. Therefore, the broken-bond model for the $DX$ center is supported. Yet, since the value of $\Delta E$ is small, the state described by the on-site model might be detected in thermal nonequilibrium samples.

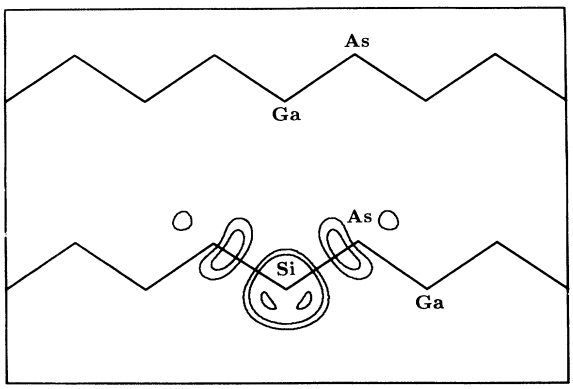


FIG. 3. The charge density of the gap level in $(Si_{Ga})^{-1}$ on the $(1\bar{1}0)$ plane. The values of the contours are $0.02\times2^n$ $e$/(a.u.)$^3$, where $n=0$–2.

Why the broken-bond and on-site geometries have similar total energies is understood in terms of the chemical-bond theory. In the broken-bond model, one Si-As $\sigma$ bond is missing compared with the on-site

geometry. This missing bond induces the large energy cost in the broken-bond geometry. On the other hand, the two electrons occupying the gap level in the negative-charge on-site geometry cause energy cost, because the wave function of the gap level has localized antibonding character. Since the wave function is mainly distributed around the Si—As bonds, the two electrons in the gap level are expected to induce an energy cost which is approximately equal to that raised by breaking one Si—As $\sigma$ bond (in general, two electrons in an antibonding level induce an energy cost which corresponds to that from breaking one bond). It is thus expected that the two geometries have similar energies.

### C. Shallow state: $D^0$

We calculate the geometry for the shallow state $D^0$ in order to investigate the difference in geometry from the negative-charge on-site model. Since the wave function of the shallow level is delocalized, the electron in the level is expected to have only a weak effect on the geometry. Thus in actual supercell calculations for $D^0$ we take the positive-charge state. We perform the 32-site cell calculations with 8- and 12-Ry cutoff energies and 64-site cell calculations with 8- and 10-Ry cutoff energies. The obtained bond lengths agree within an accuracy of 0.02 Å and thus are reliable(Table IV).

The bond length between the Si and As atoms determined from the 64-site cell calculation is 2.41 Å. It is identical to the Si-As bond length of the broken-bond geometry and is much shorter than that of the corresponding value (2.53 Å) in the on-site model. Since the long bond length in the on-site model is induced by the two electrons in the gap level, the feature for the bond lengths in the three geometries is expected to be general for the group-IV donors in GaAs. In order to examine this expectation, we perform calculations also for the Sn-related *DX* center. The 32-site cell model and 8 Ry for the cutoff energy are used. The calculated Sn-As bond length for the broken-bond model is 2.59 Å, which is identical to the calculated bond length in the shallow state, while the bond length in the on-site model is much longer (2.64 Å). It is also noted that the neutral on-site geometry with the localized wave function of the gap level has the Sn-As bond length of 2.61 Å, which is 0.02 Å longer than that of the shallow center. On the other hand, the EXAFS measurement by Hayes *et al.*[34] for the Sn impurity in $Al_xGa_{1-x}As$ shows that the Sn-As bond lengths (2.58 Å) in both the shallow state and the *DX* center are identical. This experimental result is consistent with the broken-bond model for the *DX* center. Hayes *et al.*[34] concluded, however, from the analysis of the EXAFS data that the coordination number around the Sn impurity is 4. This coordination number is inconsistent with the broken-bond model.

### D. Transition state: $[(Si_I V_{Ga})^{-1}]^*$

We discuss the emission barrier for the negatively charged broken-bond geometry from the 32-site cell calculation with 12-Ry cutoff energy. The geometries of the transition state and the broken-bond model are optimized by fixing the seven boundary Ga atoms in the supercell at the lattice sites.[48] In the optimized geometry of the transition state, the Si atom is displaced from the lattice site by 0.64 Å along the $[\bar{1}\,\bar{1}\,\bar{1}]$ axis and the Si-As bond angle is 119.5°. The amount of the distortion of the Si atom is 26% of the crystal bond length, and the obtained bond angle indicates that the hybridization is $sp^{2.0}$ (see the Appendix). Thus the energy increases from the stable broken-bond geometry to the transition state correspond to the hybridization variation from $sp^{2.4}$ to $sp^{2.0}$. This instability of the $sp^{2.0}$ hybridization is similar to that in the $NH_3$ molecule. The energy barrier for the electron emission from the broken-bond geometry, i.e., the total energy of the transition state measured from that of the broken-bond geometry, is found to be 0.30 eV. This value is comparable with observed emission barriers[7,49,50] for the *DX* center in pressured and heavily doped GaAs ($0.33\pm0.02$ eV). It is noted that Zhang[27] and DSS (Ref. 28) estimated from a LDA calculation the barrier height to be 0.22 and 0.5 eV, respectively.

Next, we treat the neutral charge state by performing calculations with various sizes. We find from the 32-site cell calculation with 12-Ry cutoff energy that the broken-bond geometry is unstable and that there is no barrier between the on-site and broken-bond geometries. This result is very sensitive to calculational parameters. In the case of the 32-site cell calculation with 8-Ry cutoff energy, there is a barrier if we take only the $\Gamma$ point as the sampling point for the Brillouin-zone integration. On the other hand, the barrier disappears if four $k$ points are taken in the calculation. The instability of the neutral broken-bond geometry is finally confirmed from the 64-site cell calculation with 10-Ry cutoff energy (four $k$ points are used in this calculation). This instability suggests that the Si atom moves to the substitutional site after the *DX* center is photoexited. The energy of the neutral on-site geometry $(Si_{Ga})^0$ with the localized state is estimated to be much lower (1.48 eV) than that of the neutral broken-bond geometry (the 32-site cell calculation with 8-Ry cutoff energy is performed). The considerably lower energy of the neutral on-site geometry is induced by annihilation of one of the electrons occupying the gap level with the localized antibonding character.

The reason for the different results among the LDA calculations by CC, DSS, and YSO is not clear at present. Yet we mention the following two points. One is the calculational parameters. As is stated above, the metastability of the neutral broken-bond geometry disappears by improving the Brillouin-zone integration. Thus, we really have to be careful about the convergence of the calculational parameters. The other point is the lattice relaxation. The present calculation includes the lattice relaxation of more than 50 atoms around the impurity. This medium-range lattice relaxation affects the total energy by more than 0.1 eV. It is thus important to include the lattice relaxation to discuss the energetics of the *DX* center.

### E. Other geometries with large lattice relaxation

We find several metastable geometries accompanied with large lattice relaxation. In this section, we present

results of the 32-site cell calculations with 8-Ry cutoff energy. In one metastable geometry $(As_{Ga}Si_{As})^{-1}$, the Si and one of the nearest-neighbor As atoms exchange their positions. Morgan proposed from an empirical calculation that this geometry is the microscopic origin of the *DX* center.[51] The present calculation, however, provides the result that this geometry has 0.6-eV higher energy than the negatively charged broken-bond geometry. In the other geometries $(Si_{Ga}Ga_I'V_{Ga'})^{-1}$, one of the second-nearest Ga atoms is distorted and becomes threefold coordinated. This Ga atom is bonded to three kinds of As atoms: the first-, third-, and fifth-nearest-neighbor As atoms from the substitutional site.[33] Thus there exist three types of breaking of the Ga—As bond, leading to three kinds of geometries for $(Si_{Ga}Ga_I'V_{Ga'})^{-1}$. The total energies of these three kinds of geometries are 0.7–0.9 eV higher than the negatively charged broken-bond geometry. Therefore we conclude that the broken-bond geometry has the lowest energy among the geometries accompanied with large lattice relaxation.

### F. Local vibrational frequency

In this section, the local vibrational frequencies of GaAs:Si are calculated at zero pressure based on the 32-site cell model with 12-Ry cutoff energy. The cutoff energy provides the converged results for the second derivative of the total energy with respect to the nuclear coordinate (see Sec. III). We estimate the frequency by considering the motion of Si and its nearest As atoms along the Si-As bond-stretching direction: the motion of the surrounding atoms is neglected. This approximation is accompanied by some error but provides qualitatively reliable results for the bond-stretching mode. For instance, as for the infrared-active Si-O bond-stretching mode for interstitial oxygen in Si, a similar calculational technique,[52] in which we take the motion of the oxygen atom and its nearest two Si atoms, gives the frequency of 1187 $cm^{-1}$, while the experimental value is 1106 $cm^{-1}$.

The calculational results for GaAs:Si are tabulated in Table V. The calculated frequency of the $t_2$ mode in the shallow state ($D^0$) is 370 $cm^{-1}$, which is in fairly good agreement with the experimental value (384 $cm^{-1}$). The vibrational frequency, which is slightly lower than that in the shallow center, is measured by Wolk *et al.*,[32] who perform the Fourier-transform infrared-absorption method under some high pressures. The extrapolated value of the frequency to zero pressure is 376 $cm^{-1}$, which is only 8 $cm^{-1}$ lower than that in the shallow center. The calculated frequency of the $t_2$ mode in the negatively charged on-site geometry, $(Si_{Ga})^{-1}$, is 301 $cm^{-1}$, which is much lower (69 $cm^{-1}$) than that in the shallow center. This considerably lower frequency is attributed to the fact that the two electrons in the gap level weaken the Si—As bonds. On the other hand, the frequency of the $t_2$ mode in the neutral on-site geometry $(Si_{Ga})^0$ is 336 $cm^{-1}$, which is 34 $cm^{-1}$ lower than that in the shallow center. By taking into account the accuracy of the present calculation, this mode may be a candidate for the observed mode. Indeed, by performing far-infrared magneto-optical and luminescence experiments, Dmochowski *et al.*[53] found the localized $a_1$ state for the Si impurity under high pressure. However, Wolk *et al.*[32] concluded from infrared-absorption and Hall-effect measurements that the impurity inducing the detected infrared-absorption peak is negatively charged. Thus, the neutral on-site model is inconsistent with the measurements for the charge state.

Here we emphasize that the *e* mode of the broken-bond geometry, $(Si_IV_{Ga})^{-1}$, is another candidate for the detected mode: The calculated frequency (392 $cm^{-1}$) is close to that in the shallow center (see Table V). As mentioned in a previous paper,[33] similar frequencies of the shallow center and of the broken-bond geometry are due to the fact that bond strengths are close to each other (the bond lengths in both geometries are very close to each other). The calculated frequency of the *e* mode is slightly (22 $cm^{-1}$) higher than the shallow center. Actually, this result of the higher frequency of the *e* mode is inconsistent with the experimental one (the detected peak is located in the slightly lower-frequency region than the peak of the shallow center). However, the motion of the surrounding atoms, which is not included in the present calculation, is likely to lower the frequency of the *e* mode. Thus, in order to determine whether the observed mode is the $t_2$ mode of the neutral on-site geometry or the *e* mode of the broken-bond geometry, we should take into account the effect of the surrounding atoms by evaluating the dynamical matrix of all the atoms.

Jones and Öberg previously calculated the local vibrational frequencies by using a cluster model and by considering the motion of the surrounding atoms. Their calcu-

TABLE V. Infrared-light-absorption-active local vibrational frequencies in $cm^{-1}$. The calculations are performed for $(Si_IV_{Ga})^{-1}$, $(Si_{Ga})^{-1}$, $(Si_{Ga})^0$, and $D^0$ geometries. The values in parentheses are the differences from the frequency of the shallow center.

| | $D^0$ | *DX* center | $(Si_IV_{Ga})^{-1}$ | | $(Si_{Ga})^{-1}$ | $(Si_{Ga})^0$ |
|---|---|---|---|---|---|---|
| | $t_2$ | | *e* | $a_1$ | $t_2$ | $t_2$ |
| Experiment (Ref. 32) | 384 | 376 (−8) | | | | |
| Present work | 370 | | 392 (+22) | 274 (−96) | 301 (−69) | 336 (−34) |
| Jones and Öberg | 386 | | 432 (+46) | [a] | 347 (−39) | |

[a]The frequency of the mode is located in the one-phonon band.

lated frequency of the $e$ mode of the broken-bond geometry is 432 $cm^{-1}$, which is 46 $cm^{-1}$ higher than that of the shallow center. We speculate that the calculated much-higher frequency of the $e$ mode originates from the optimized geometry from their cluster calculations: In the geometry, the Si-As bond length is 2.33 Å, while the present value is 2.42 Å.

Finally, our calculation predicts the existence of the low-frequency peak (274 $cm^{-1}$) due to the $a_1$ mode in the broken-bond model (see Table V). Considering the calculational error, the peak might appear in the position which is higher than the frequency (292 $cm^{-1}$) (Ref. 45) of the longitude-optical (LO) phonon at the $\Gamma$ point. In this case, the peak is sharp and detectable. If the peak is below the LO phonon frequency, however, the distribution of the absorption intensity around the peak becomes broad. Furthermore, samples are totally reflective in the region between the LO and TO phonon frequencies at the $\Gamma$ point. Thus the peak would be difficult to detect. In any case, if the low-frequency peak is detected from the infrared-light-absorption measurement under the condition that the *DX* level appears, it would be clear evidence for the broken-bond model.

## V. CONCLUSION

We have performed a supercell calculation for GaAs:Si by using the norm-conserving pseudopotential method within the LDA. Several geometries of GaAs:Si are optimized by taking into account the relaxation of all the atoms in the unit cell. As a result, we obtain the following results for this impurity. The Si—As bonds in the broken-bond geometry, $(Si_I V_{Ga})^{-1}$, are stabilized by the $sp^{2.4}$ hybridization of the Si atomic orbitals, while the Si—As bonds in the negatively charged on-site geometry, $(Si_{Ga})^{-1}$, are weakened by the electrons in the gap level with the localized antibonding character. Thus, the bond lengths in the two geometries are very different: the bond lengths are 2.41 and 2.53 Å in the broken-bond and on-site geometries, respectively. It is interesting that the former bond length is identical to the calculated value for the shallow state. This characteristic feature of the bond lengths for the three geometries is also found in the case of the Sn donor: we find from the calculations with the 32-site cell model that the bond length (2.59 Å) in the shallow state is identical to that in the broken-bond geometry, while the bond length (2.64 Å) in the negatively charged on-site model is much longer. Therefore, the result of the EXAFS measurements that the bond lengths of the shallow and *DX* levels are identical (2.58 Å) seems to support the broken-bond model.

Furthermore, we obtain the following findings for GaAs:Si: the total energy in the broken-bond geometry, $(Si_I V_{Ga})^{-1}$, is slightly lower than that in the on-site one, $(Si_{Ga})^{-1}$, supporting the broken-bond model. In addition, the broken-bond geometry is found to have the lowest energy among the geometries accompanied by large lattice relaxation. The emission barrier for the broken-bond geometry is estimated to be 0.30 eV, which is consistent with the experimental value (0.33±0.02 eV) for the *DX* center. The hybridization character at the transition state, $[(Si_I V_{Ga})^{-1}]^*$, is found to be close to $sp^2$, and is in contrast with $sp^{2.4}$ in the stable broken-bond geometry. The local vibrational frequency in the negatively charged on-site model, $(Si_{Ga})^{-1}$, is much lower than the observed value of the Si-impurity local vibrational mode appearing under high pressure. This considerably lower frequency is due to the fact that the Si—As bonds are weakened by the electrons in the gap level. It is concluded that the observed mode is the $e$ mode in the broken-bond model or the $t_2$ mode in the neutral on-site model $(Si_{Ga})^0$. Most of the calculational results in this study support the broken-bond model for the *DX* center. Finally, we find drastic variation of the potential surface between the neutral and negative charges: the neutral broken-bond geometry is unstable and there is no barrier between the on-site and broken-bond geometries. These findings suggest that the Si atom moves to the substitutional site after the *DX* center is photoexcited.

## APPENDIX: ANALYSIS OF HYBRIDIZATION

In this appendix, we analyze the Si-As bond character in the optimized broken-bond geometry. In general, the Si $sp^a$ hybridization orbitals for the Si-As bonds are given by

$$|i\rangle = |s\rangle + \sqrt{a}\,|p_i\rangle\ , \tag{A1}$$

where $|s\rangle$ and $|p_i\rangle$ are the Si $s$ and $p$ orbitals, respectively and $i$ indicates the sequential number of the Si-As bonds. In the above equation, the normalization constant is omitted for simplicity. It is assumed that the direction of the $p$ orbital in the above equation is parallel to the bond axis. Since the present supercell calculation determines that the Si-As bond angle is 115° (see Sec. IV), we take the value of 115° for the angle between each two of the three $p$ orbitals in (A1). Then the condition that the above three hybridized orbitals must be orthogonal to each other leads to the conclusion that the value of $a$ is 2.4. Thus the hybridization in the Si atom in the optimized geometry of $(Si_I V_{Ga})^{-1}$ is $sp^{2.4}$, i.e., something between $sp^2$ and $sp^3$. Next the Si dangling bond orbital is given by

$$|4\rangle = |s\rangle + \sqrt{b}\,|p_{[\bar{1}\bar{1}\bar{1}]}\rangle\ , \tag{A2}$$

where the $p_{[\bar{1}\bar{1}\bar{1}]}$ orbital is in the direction of the $[\bar{1}\,\bar{1}\,\bar{1}]$ axis. According to the optimized atomic geometry from the supercell calculation, the angle between the bonds in (A1) and (A2) is 103.5°. Since the orbitals in (A1) and (A2) are orthogonal, the value of $b$ must be 7.9 and consequently the hybridization is $sp^{7.9}$, indicating that the character of the dangling bond is between $sp^3$ and $p_\pi(sp^\infty)$. Similarly, as for $[(Si_I V_{Ga})^{-1}]^*$, the Si-As bond character is $sp^{2.0}$ (the bond angle is 119.5°).

[1]For a review, see T. N. Theis, in *Proceedings of the Fourteenth International Symposium on Gallium Arsenide and Related Compounds,* edited by A. Christou and H. S. Rupprecht, IOP Conf. Proc. No. 91 (Institute of Physics and Physical Society, London, 1988), p. 1; M. Mizuta, in *Proceedings of International Conference on Science and Technology of Defect Control in Semiconductors, Yokohama, Japan,* edited by K. Sumino (Elsevier, Amsterdam, 1990), p. 1043.

[2]D. V. Lang and R. A. Logan, Phys. Rev. Lett. **39**, 635 (1977); D. V. Lang, R. A. Logan, and M. Jaros, Phys. Rev. B **19**, 1015 (1979).

[3]N. Lifshitz, A. Jayaraman, and R. A. Logan, Phys. Rev. B **21**, 670 (1980).

[4]T. Baba, T. Mizutani, and M. Ogawa, Jpn. J. Appl. Phys. **22**, L627 (1983).

[5]N. Chand, T. Henderson, J. Klem, W. T. Masselink, R. Fischer, Yia-C. Chang, and H. Morkoç, Phys. Rev. B **30**, 4481 (1984).

[6]E. F. Schubert and K. Ploog, Phys. Rev. B **30**, 7021 (1984).

[7]M. Mizuta, M. Tachikawa, H. Kukimoto, and S. Minomura, Jpn. J. Appl. Phys. **24**, L143 (1985).

[8]M. Tachikawa, T. Fujisawa, H. Kukimoto, A. Shibata, G. Oomi, and S. Minomura, Jpn. J. Appl. Phys. **24**, L893 (1985).

[9]E. Calleja, P. M. Mooney, S. L. Wright, and M. Heiblum, Appl. Phys. Lett. **49**, 1542 (1986).

[10]T. N. Theis, B. D. Parker, P. M. Solomon, and S. L. Wright, Appl. Phys. Lett. **49**, 1542 (1986).

[11]R. Legros, P. M. Mooney, and S. L. Wright, Phys. Rev. B **35**, 7505 (1987).

[12]D. K. Maude, J. C. Portal, L. Dmowski, T. Foster, L. Eaves, M. Nathan, M. Heiblum, J. J. Harris, and R. B. Beall, Phys. Rev. Lett. **59**, 815 (1987).

[13]M. F. Li, P. Y. Yu, E. R. Weber, and W. Hansen, Appl. Phys. Lett. **51**, 349 (1987).

[14]M. F. Li, P. Y. Yu, E. R. Weber, and W. Hansen, Phys. Rev. B **36**, 4531 (1987).

[15]P. M. Mooney, N. S. Caswell, and S. L. Wright, J. Appl. Phys. **62**, 4786 (1987).

[16]T. N. Theis, P. M. Mooney, and S. L. Wright, Phys. Rev. Lett. **60**, 361 (1988).

[17]P. M. Mooney, G. A. Northrop, T. N. Morgan, and H. G. Grimmeiss, Phys. Rev. B **37**, 8298 (1988).

[18]A. K. Saxena, Solid State Electron. **25**, 127 (1982).

[19]T. N. Morgan, Phys. Rev. B **34**, 2664 (1986).

[20]A. Oshiyama and S. Ohnishi, Phys. Rev. B **33**, 4320 (1986).

[21]H. P. Hjalmarsom and T. J. Drummond, Phys. Rev. Lett. **60**, 2410 (1988).

[22]Y. Mochizuki, M. Mizuta, and A. Oshiyama, Jpn. J. Appl. Phys. **29**, 1530 (1990).

[23]J. C. Bourgoin, S. L. Feng, and H. J. von Bardeleben, Phys. Rev. B **40**, 7663 (1989).

[24]T. Fujisawa, J. Yoshino, and H. Kukimoto, Jpn. J. Appl. Phys. **29**, L388 (1989).

[25]D. J. Chadi and K. J. Chang, Phys. Rev. Lett. **61**, 873 (1988); Phys. Rev. B **39**, 10063 (1989).

[26]S. B. Zhang and D. J. Chadi, Phys. Rev. B **42**, 7174 (1990).

[27]S. B. Zhang, Phys. Rev. B **44**, 3417 (1991).

[28]J. Dabrowski, M. Scheffler, and R. Strehlow, in *Proceedings of the 20th International Conference on the Physics of Semiconductors, Thessaloniki, Greece, 1990,* edited by E. M. Anastassakis and J. D. Joannopoulos (World Scientific, Singapore, 1990), p. 489.

[29]E. Yamaguchi, K. Shiraishi, and T. Ohno, J. Phys. Soc. Jpn. **60**, 3093 (1991); in *Proceedings of the 20th International Conference on the Physics of Semiconductors* (Ref. 28), p. 501.

[30]G. A. Baraff, Semicond. Sci. Technol. B **6**, 9 (1991).

[31]R. Jones and S. Öberg, Phys. Rev. B **44**, 3407 (1991).

[32]J. A. Wolk, M. B. Kruger, J. N. Heyman, W. Walukiewicz, R. Jeanloz, and E. E. Haller, Phys. Rev. Lett. **66**, 774 (1991).

[33]M. Saito, A. Oshiyama, and O. Sugino, Phys. Rev. B **45**, 13745 (1992).

[34]T. M. Hayes, D. L. Williamson, A. Outzourhit, P. Small, P. Gibart, and A. Rudra, J. Electron. Mater. **18**, 207 (1989).

[35]A. Oshiyama and M. Saito, J. Phys. Soc. Jpn. **56**, 2104 (1987); Phys. Rev. B **36**, 6156 (1987).

[36]O. Sugino and A. Oshiyama, in *Proceedings of the 16th International Conferences on Defects in Semiconductors, Lehigh, PA, 1991,* edited by G. Davies, G. G. Deleo, and M. Stavola (Trans Tech, Aedermannsdorf, 1991), p. 469; unpublished.

[37]R. Car and M. Parrinello, Phys. Rev. Lett. **55**, 2417 (1985).

[38]M. Teter, M. Payne, and D. Allan, Phys. Rev. B **40**, 12255 (1989); D. M. Bylander, L. Kleinman, and S. Lee, *ibid.* **42**, 1394 (1990).

[39]L. Kleinman and D. M. Bylander, Phys. Rev. Lett. **48**, 1425 (1982).

[40]M. Saito, O. Sugino, and A. Oshiyama, Phys. Rev. B **46**, 2606 (1992).

[41]X. Gonze, R. Stumpf, and M. Scheffler, Phys. Rev. B **44**, 8503 (1991).

[42]A. Baldereschi, Phys. Rev. B **7**, 5212 (1973).

[43]D. J. Chadi and M. L. Cohen, Phys. Rev. B **8**, 5747 (1973).

[44]G. Nilsson and G. Nelin, Phys. Rev. B **6**, 3777 (1972).

[45]D. Strauch and B. Dorner, J. Phys. Condens. Matter **2**, 1457 (1990).

[46]The calculated charge densities of electrons in the gap level by CC (Ref. 25) and Zhang (Ref. 27) show that the Si atom has a $s$-$p$ hybridized dangling-bond orbital. Thus, their calculational results also suggest that the Si-As bond character is not pure $sp^2$.

[47]M. Saito and A. Oshiyama (unpublished).

[48]This restriction for the geometry optimization increases the energy of the broken-bond geometry by 0.10 eV.

[49]P. M. Mooney, T. N. Theis, and S. L. Wright, Appl. Phys. Lett. **53**, 2546 (1988).

[50]T. Baba, M. Mizuta, T. Fujisawa, J. Yoshino, and H. Kukimoto, Jpn. J. Appl. Phys. **28**, L891 (1989).

[51]T. N. Morgan, Semicond. Sci. Technol. **6**, B23 (1991).

[52]M. Saito and A. Oshiyama, Phys. Rev. B **38**, 10711 (1988).

[53]J. E. Dmochowski, P. D. Wang, R. A. Stradling, and W.Trzeciakowski, in *Proceedings of the 16th International Conference on Defects in Semiconductors* (Ref. 36), p. 751.